DOI: 10.19884/j.1672-5220.202502016

Theory and Practice of Multi-Fiber Blending Carding with Fully Fixed Flat

SONG Xinyu[1], DAI Xianlei[2], ZHANG Shufeng[3], XUE Wenliang[1*], CHENG Longdi[1]
1. Key Laboratory of Textile Science & Technology, Ministry of Education, College of Textiles, Donghua University, Shanghai 201620, China
2. Jinfeng Textile Machinery, Wenzhou 325041, China
3. Longrun Textile Co. Ltd., Zaozhuang 277400, China

Abstract: To investigate the differences in the carding effect between fully fixed flat carding machines and movable flat carding machines, this study employed the Fluent software to conduct numerical simulations of airflow velocity distributions between the cylinder and flat of both machine types, with particular focus on analyzing the airflow patterns near microscopic needle teeth. The simulation results were further verified by practical carding and spinning experiments of multi-fibers, namely diacetate, viscose, heat-shrinkable acrylic, micro-denier acrylic and wool fibers. The results demonstrate that the fully fixed flat carding machine exhibits a more stable airflow boundary layer near the needle teeth, which enhances the carding effect as evidenced by improved yarn quality parameters.

Keywords: carding machine; fully fixed flat; multi-fiber blending; simulation
CLC number: TS103.221 **Document code**: A
Article ID: 1672-5220(2026)04-0041-08

0 Introduction

Carding is a crucial step in the spinning process, often referred to as the heart of spinning[1]. With the rapid advancement of the textile industry, the production rate of carding machines has also increased significantly[2]. Over recent decades, other core components have undergone structural optimizations to accommodate the high-yield operation of modern carding machines. However, the movable flat, one of the key elements affecting carding quality, has seen only limited improvement in terms of the carding effect over the past decades. This is primarily due to the use of elastic card clothing in movable flat carding machines, which features a high needle height and a thin elastic base fabric that suffers from issues related to firmness and durability. These limitations restrict further increases in the carding machine production rate[3]. In contrast, the fully fixed flat carding machine employs metal card clothing which has a lower needle height and higher needle density, enabling it to achieve gradual carding. This design improves both output and carding quality[4].

Due to the viscosity of air, frictional resistance is generated during airflow movement. When the cylinder rotates at a high speed, an attached layer forms on its surface, which is defined as the boundary layer. This boundary layer plays a crucial role in breaking down fiber bundles into single fibers and removing corresponding impurities. Notably, it has been demonstrated that changes in the cylinder tooth structure affect the carding airflow in the main carding area, by a numerical simulation of the carding zone with an elastic flat[5-6]. Consequently, alterations in the card clothing may similarly influence the adjacent flow field dynamics. The carding machine facilitates the transformation of raw materials into discrete fibers, while the airflow between the cylinder and flat directly governs fiber trajectory[7]. Although several experimental studies have been conducted on fully fixed flat carding machines[8-11], a systematic analysis of airflow characteristics remains unexplored. This study analyzes and compares the differences in the airflow between the cylinder and flat in two types of carding machines, and its impact on the carding effect, based on numerical simulation results.

As market demand and technological advancements increase, the use of chemical fibers in textiles has gained significant attention. The multi-fiber blending can meet the wearability specified by the final product customer. Diacetate fibers demonstrate relatively low tensile strengths owing to the reduced crystallinity and molecular orientation, which makes them particularly suitable as the primary component in blended yarns for assessing fiber stress distribution during processing in a fully fixed flat carding machine. In this study, a carefully designed blended yarn comprising diacetate, viscose, heat-shrinkable acrylic, micro-denier acrylic, and wool fibers is developed. The diacetate fiber provides the resultant fabric with desirable luster and dimensional stability, while the combination of micro-denier and heat-shrinkable acrylic fibers contributes to enhanced bulkiness and

Received date: 2025-02-27
* Correspondence should be addressed to XUE Wenliang, email: xwl@dhu.edu.cn
Citation: Song X Y, Dai X L, Zhang S F, et al. Theory and practice of multi-fiber blending carding with fully fixed flat[J]. *Journal of Donghua University (English Edition)*, 2026, 43(4): 41-48.

softness. Furthermore, the inherent crimp structure of wool fibers creates insulating air pockets that effectively manage moisture by rapidly absorbing and transporting perspiration away from the skin surface, thereby optimizing wearer comfort. This multi-fiber blending strategy serves dual purposes: it facilitates comprehensive evaluation of the carding mechanism in the fully fixed flat carding system and simultaneously ensures superior functional performance in the end-use textiles, thus successfully bridging fundamental research with practical textile engineering considerations. The mass ratio of diacetate, viscose, heat-shrinkable acrylic, micro-denier acrylic, and wool is 36 ∶ 30 ∶ 20 ∶ 10 ∶ 4. Yarns with a linear density of 14.76 tex are produced using both the fully fixed flat carding machine and movable flat carding machine. Performance tests and comparative analyses of the semi-finished raw strip and final yarn are conducted to evaluate the feasibility of applying the fully fixed flat carding machine to the differentiated blended fibers. The study would provide both theoretical and practical insights for the use of the fully fixed flat carding machine.

1 Numerical Computation

1.1 Model construction and boundary conditions

The three-dimensional (3D) structures and positions of the cylinder and flat for both carding machines are shown in Figs. 1 and 2, where the upper part of each model represents a partial flat with dimensions of 30 mm in both length and width. In the movable flat carding machine, the elastic card clothing features U-shaped comb needles with a height of 7.9 mm arranged in a 4 × 6 twill pattern. By contrast, the metal card clothing of the fully fixed flat carding machine adopts the commercially prevalent and commonly used specifications for carding processes. The lower part of the model represents a segment of the cylinder, which has an overall diameter of 1 288 mm, with the modeled section also measuring 30 mm in length and width. The cylinder model is symmetrically positioned on both sides, while the flat model is slightly inclined, with an inlet clearance of 0.9 mm and an outlet clearance of 0.3 mm between the cylinder and flat.

As shown in Figs. 1 and 2, a space exists between the cylinder and flat of the carding machine. As previously discussed, the viscous airflow generates a boundary layer in this space when the cylinder rotates at a high speed. This boundary layer triggers Taylor vortex-like motion along the flat surface, forming an airflow boundary layer within the cylinder-flat space. However, the axial airflow between the metal needles and the flat suppresses the development of the Taylor vortices[12].

This study models the airflow between the cylinder and flat by using the computational domain obtained through Boolean subtraction of the solid components, with the entire airflow field divided into upper and lower subregions connected by an interface for data transfer. During the carding process, the high-speed rotation of the cylinder creates an airflow boundary layer on its surface, making the airflow between the cylinder and flat a high-speed, compressible, and viscous turbulent airflow. Considering that the realizable k-ε turbulence model demonstrates superior accuracy and reliability in simulating strong swirling airflows, this model is selected for the numerical simulations in this work.

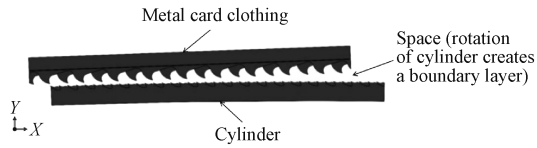


Fig. 1 Physical model between cylinder and flat of fully fixed flat carding machine

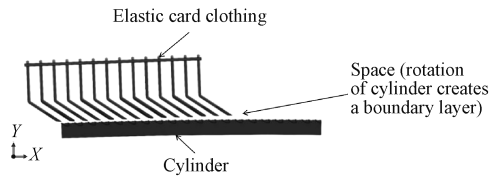


Fig. 2 Physical model between cylinder and flat of movable flat carding machine

The numerical simulation was performed with the external airflow boundary defined as atmospheric pressure. The rotating cylinder domain was modelled by using a dynamic mesh rotating about its central axis for transient flow analysis. A time step size of 1×10^{-7} s was employed for 10 000 iterations, with the modified semi-implicit method for pressure-linked equations consistent (SIMPLEC) algorithm being implemented to enhance the computational effect. The solution convergence criterion was set to 1×10^{-3} to ensure the solution accuracy while maintaining reasonable computation time.

1.2 Mesh generation

The computational domain was discretized by using Fluent Meshing with a multi-block grid generation approach. To accurately resolve the flow characteristics near the needle teeth regions, local grid refinement was applied to both the cylinder and flat needle zones with a mesh size of 0.004 mm, ensuring precise capture of the intricate flow patterns in these critical areas. The effect of grid resolution on airflow velocity is presented in Fig. 3.

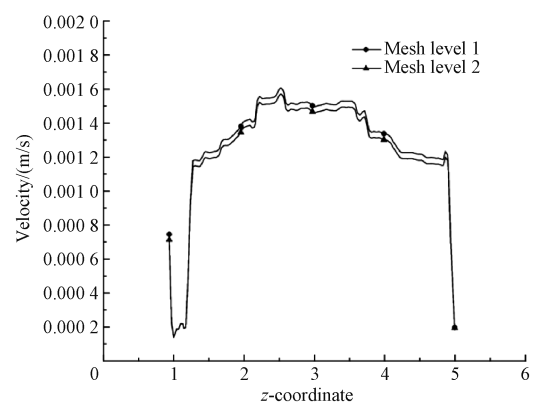


Fig. 3 Effect of grid resolution on airflow velocity

The computational mesh was refined locally around the cylinder and flat needle teeth to accurately resolve the microscopic airflow characteristics in these critical regions, while employing coarser elements in the remaining domains to optimize the computational efficiency. A grid independence verification was performed on the movable flat configuration using two distinct mesh density levels, with a total element count of 5 309 158 (mesh level 1) and 5 803 788 (mesh level 2), respectively.

The velocity profiles exhibit minor variations between mesh level 1 and mesh level 2. Based on a comprehensive consideration of the computational effect and solution accuracy, mesh level 1 was selected for the numerical simulations in this study. The mesh generation results are presented in Fig. 4.

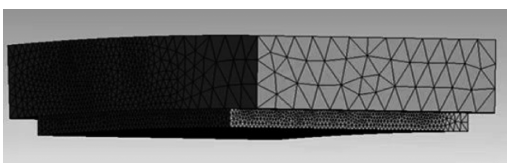


Fig. 4 Airflow field mesh generation

The velocity contour plot on the YZ plane at $X = -0.012$ m was extracted, with its corresponding location in the geometric configuration illustrated in Fig. 5.



Fig. 5 Schematic diagram of airflow analysis data extraction location (a is extraction location of metal card clothing; b is extraction location of elastic card clothing)

Figure 6 shows the velocity distribution of the extracted airflow. The airflow generated by the rotation of the cylinder forms a surface layer, which is disrupted by the needle teeth on the flat, creating a velocity trough near the needle teeth. The width of the airflow near the metal card clothing is narrower than that near the elastic card clothing, and the velocity difference of the airflow is lower, increasing the number of fibers affected by the airflow in that region.

For fibers moving within the airflow field, let the velocity of the fibers be denoted as v_t. Consider a differential segment dl of the fiber, at which the air velocity is v. The force F exerted by the airflow on this segment is

$$F = \frac{1}{2} C_d \rho (v - v_t)^2 d_f \mathrm{d}l \sin\theta, \qquad (1)$$

where C_d is the coefficient of friction; ρ is the air density; d_f is the diameter of the fiber; θ is the angle between the fiber and the tangent to the streamline.

The fibers on the elastic needle teeth had a wider surface layer attached to the airflow, causing more fibers to move in the axial direction of the teeth. Additionally, due to the higher velocity difference between the airflow and the surface layer, the transverse force on the fibers was higher, leading to a larger displacement. As a result, there were more lateral connections between the fibers, resulting in more neps.

The velocity color in Fig. 6 is derived from numerical simulation results, where the white rectangular regions represent the tips of card needle teeth, and the rest of the domain corresponds to the airflow boundary layer adjacent to the needle teeth. In the length direction, corresponding to the cylinder's axial direction, the fully fixed flat demonstrates the lowest airflow boundary layer velocity, with the movable flat exhibiting intermediate values. This phenomenon occurs because the movable flat is equipped with elastic card clothing which features a low axial needle density and low airflow resistance, thereby forming a higher-velocity boundary layer. The enhanced axial airflow velocity between the cylinder and flat increases forces acting on fibers, promoting transverse fiber movement and inter-fiber interactions that contribute to nep formation.

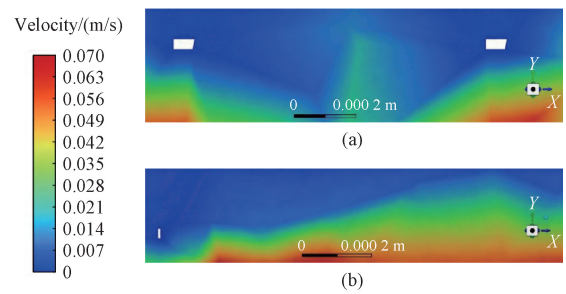


Fig. 6 Diagram of airflow velocity distribution between cylinder and flat: (a) fully fixed flat carding machine; (b) movable flat carding machine

Consistent airflow field variations can also be identified along the transverse vertical direction. A prominent contrast exists between the fully fixed flat and movable flat: the airflow boundary layer attached to the fully fixed flat is markedly thinner, whereas a substantially wider boundary layer develops around the movable flat equipped with elastic card clothing. Such airflow boundary layer distribution characteristics originate from the structural differences between metal card clothing and elastic card clothing. Elastic needle teeth on movable flats are higher with a thinner base fabric, which collectively increases the effective airflow clearance. Under the thin boundary layer condition of the fully fixed flat, the centrifugal force compels fibers to make frequent contact with the needle teeth in the carding zone. The resulting mechanical traction and aerodynamic drag further promote fiber straightening and parallelization.

The resulting increase in overall fiber tension improves fiber alignment and straightening, thereby enhancing the carding intensity and effectiveness. However, this benefit comes with a trade-off: when the induced tension exceeds individual fibers' breaking load, it may cause fiber damage and elevate short fiber content in the final product. These findings highlight the critical balance between achieving optimal carding performance and maintaining fiber quality through proper flat selection and operation. As a result, the overall fiber tension increases, leading to greater alignment and straightening of the fibers. This enhances the carding strength and improves the carding effect. However, the increased fiber tension may also cause fiber damage, leading to a higher content of short fibers.

2 Materials and Methods

2.1 Materials and spinning process parameters

Diacetate fibers were purchased from Eastman Corporation (USA). Viscose fibers were purchased from Sanyou Yuanda Fiber Co., Ltd. (China). Heat-shrinkable acrylic fibers were purchased from Jilin Qifeng Chemical Fiber Co., Ltd. (China), and micro-denier acrylic fibers were purchased from Jilin Jimeng Acrylic Fiber Co., Ltd. (China). Australian wool fibers with a staple length of 70 mm were adopted in this study. The basic physical parameters of fibers are listed in Table 1.

Table 1 Basic physical parameters of fibers

Fiber	Length/mm	Linear density/dtex	Elongation at break/%	Breaking load/cN	Tenacity/(cN/dtex)	Moisture regain/%
Diacetate	38.00	1.20	2.41	31.39	1.81	6.20
Viscose	38.00	1.33	3.49	21.44	2.62	10.70
Heat-shrinkable acrylic	38.00	1.24	4.68	24.03	3.77	1.50
Micro-denier acrylic	38.00	0.89	3.54	35.53	3.97	1.60
Wool	82.20	3.30	5.47	44.50	1.66	12.90

In the spinning process, the model selection and process parameters were optimized based on enterprise practices, aligning with the optimal process configurations used in textile production. Carding processing was performed on two sets of FA201B carding machines (Qingdao Hongda Textile Machinery Co., Ltd., China), including a modified version equipped with a fully fixed flat and an unmodified original version fitted with a movable flat.

The diacetate/viscose/heat-shrinkable acrylic/micro-denier acrylic/wool blended yarns were spun under identical conditions, with other process parameters and spinning processes kept constant. For each sample, 20 bobbins were spun for testing. A cleaning-and-carding integrated unit was used to process the raw fibers into carded slivers. Three drawing processes were employed, followed by roving and spinning processes.

A JWF1310-type drawing machine (Jingwei Textile Machinery, China) was used for both the first and the second drawing processes. The numbers of slivers for the first and second draws were 8 and 6, respectively, with a raw sliver linear density of 23 g/(5 m). For the final drawing process, an RSBD22C draw frame (Rieter, Switzerland) was then used, with 6 slivers and a sliver linear density of 21 g/(5 m). In the roving process, an FA497 suspended roving frame (Saitex Global Machinery, China) was employed, with a roving mass of 4.5 g/(10 m). The total drafting factor was 4.67, and the roving twist factor was 75. The spinning process used a JWF1510-type spinning frame, with a total drafting factor of 69.06. The detailed technical parameters of the carding machine are listed in Table 2.

Table 2 Main process parameters of carding machine

Parameter	Value
Raw sliver linear density/(g/(5 m))	23
Strip speed/(m/min)	60
Barbed roller speed/(r/min)	650
Cylinder speed/(r/min)	200
Movable flat space/(inch/1 000)	9×8×8×8×9
Fully fixed flat space/(inch/1 000)	8×9×9×10×10×12×13×17

2.2 Quality assessment

In this experiment, samples (0.5 g) were used for each machine, and the method for detecting raw sliver quality proposed by Liu et al.[13] was used. The collected raw sliver samples were manually split into uniform fiber webs from both ends, and nep defects were subsequently inspected and statistically counted. A total of 10 samples were tested, and the results were averaged. The same sampling method was used to calculate the short fiber content which was determined through hand sorting. The raw sliver produced by each carding machine was tested twice, and the average value was taken to guarantee the reliability of experimental data.

Based on GB/T 3 292.1—2008, the Uster ME100 (Uster Technologies, Switzerland) was used to determine the coefficient of mass variation (CVm), thick places (+35% and +50%), thin places (−40% and −50%), and yarn hairiness at a testing speed of 400 m/min. For example, a thin place −40% is defined as a yarn segment with a cross-sectional mass at least 40% below

the nominal linear density, and a thick place+35% refers to a yarn segment with a cross-sectional mass at least 35% above the nominal value.

The tensile properties of the yarns produced by both the fully fixed flat carding machine and movable flat carding machine were measured using the YG063G Strength Tester (Changling Textile Electromechanical Technology, China). Tensile properties were tested according to GB/T 3916—2013 at a constant rate of extension, with a pre-tension of 50 cN/tex, a gauge length of 500 mm, and a crosshead speed of 500 mm/min.

For all the above yarn quality and tensile tests, 20 bobbins were selected for each experiment, with five replicate measurements per bobbin prior to averaging.

2.3 Statistical analysis

Independent-sample *t*-tests were done to determine whether the quality of raw slivers and finished yarns differed significantly between the two carding machines. Levene's test for equality of variances was first conducted to assess the homogeneity of variance. When homogeneity was satisfied, *t*-test results based on pooled variance were adopted; otherwise, the corrected *t*-test results with separate variance and adjusted degrees of freedom were used. All statistical analyses were conducted using SPSS at a significance level of 0.05.

3 Results and Discussion

3.1 Analysis of raw strip quality

The preceding airflow-field simulation confirms that metal card clothing provides significantly better axial airflow stability than elastic card clothing, which theoretically favors fiber motion behavior. As shown in Table 3, the two carding schemes show only minor differences in the mean nep count and short-fiber content by number in the raw sliver, and these differences are not statistically significant. Local airflow turbulence primarily affects fiber movement at the microscopic scale, whereas the nep count and short-fiber content by number are macroscopic indicators of overall carding performance. These macroscopic indicators are insensitive to minor microscopic fluctuations of localized airflow, yielding trivial and statistically non-significant mean differences within the given confidence interval.

Table 3 Comparison of raw sliver quality data

Carding machine type	Nep count/(count/g)		Short-fiber content by number/%	
	Average	Significance	Average	Significance
Movable flat carding machine	8.60	0.236	8.90	0.348
Fully fixed flat carding machine	7.60		11.70	

3.2 Analysis of yarn unevenness

The yarn evenness values are shown in Fig. 7. The independent-samples *t*-test results are presented in Table 4. The yarn thickness, as well as the coefficient of variation, is not only related to the short-fiber content by number in the raw sliver, but also influenced by the degree of alignment parallel to the sliver axis[13-14]. Yarns produced with the fully fixed flat carding machine exhibit significantly lower CVm than those with the movable flat carding machine. This improvement results from the converging airflow of metal card clothing, which reduces fiber displacement in the carding zone and lowers kinematic dispersion among fibers with different properties. Consequently, fiber distribution during drafting becomes more uniform, CVm across yarn cross-sections is reduced, and evenness is significantly improved.

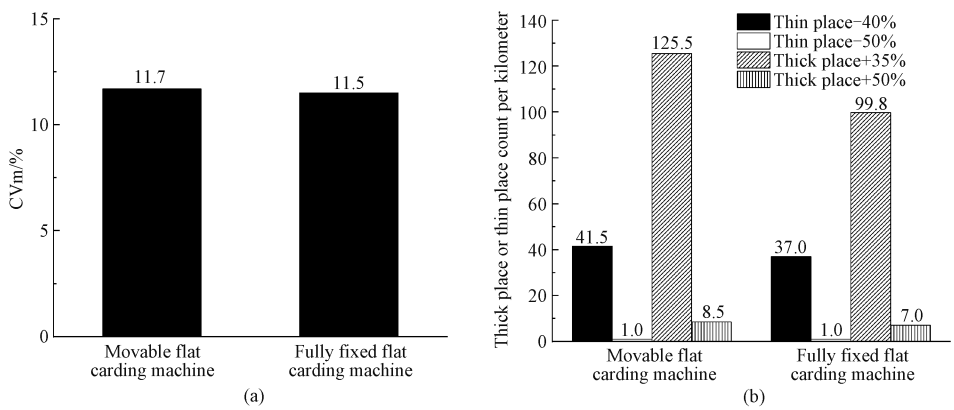


Fig. 7 Comparison of average yarn evenness: (a) CVm; (b) thick and thin places

Table 4 Independent-sample *t*-test results of yarn evenness

Parameter	Degree of freedom	Significance
CVm	38.00	<0.01*
Thin place−40%	19.00	<0.01*
Thin place−50%	24.00	0.25
Thick place+35%	36.48	<0.01*
Thick place+50%	38.00	0.42

Note: * indicates statistically significant difference at $p < 0.05$.

Thin places arise primarily from asynchronous fiber motion, uncontrolled floating fibers, differential slippage among blended fibers, and localized fiber deficiency. The thin place−40% count of yarns from the fully fixed flat carding machine is lower, with a mean dropping from 41.5 counts/km to 37.0 counts/km. The mechanism is that the substantial property differences among blended components render fibers prone to hysteresis and slippage under the divergent airflow of elastic card clothing, facilitating thin-place formation. In contrast, the converging airflow of metal card clothing imposes stronger and more uniform constraint on multi-component fibers, enhancing fiber control and reducing both slippage and localized fiber loss in the drafting zone. As for thin place−50%, such imperfections have larger diameters and are predominantly governed by the overall carding intensity and short-fiber content, with a weak correlation with the local airflow around card teeth. Meanwhile, this index has an extremely low average baseline and slight inter-group variation, resulting in no significant difference between the two schemes.

The primary causes of thick places are fiber entanglement during carding and asynchronous fiber motion during drafting, both closely related to the degree of fiber straightening, parallelization, and separation. The count of thick place+35% is also lower for the fully fixed flat carding machine, with the mean declining from 125.5 counts/km to 99.8 counts/km. This further corroborates the role of the stable axial airflow generated by metal card clothing, which effectively suppresses transverse fiber movement and oscillation along the cylinder axis. This maintains fibers in a well-straightened and parallelized state during carding, reducing collision, entanglement, and bundle formation. Improved fiber straightness, in turn, promotes more orderly fiber motion in the drafting zone and substantially reduces the number of floating fibers, thereby preventing thick places caused by uncontrolled drafting. The improvement in the thick place+50% count is not significant, as such defects predominantly arise from large unremoved fiber bundles or neps. Given that sliver testing reveals no significant difference in the nep count between the two schemes, the yarn results are consistent.

3.3 Analysis of hairiness

The hairiness of a yarn refers to the number of fiber ends protruding from its surface. It is correlated with the short-fiber content by number, and an increase in the number of short fibers typically leads to more yarn hairiness[15]. However, this is also influenced by the degree of fiber alignment in the raw sliver[16]. There is an insignificant difference in the average hairiness index between yarns processed by the fully fixed flat carding machine and the movable flat carding machine, as shown in Fig. 8 and Table 5. Combined with the foregoing numerical simulation results, the optimized fiber parallelism achieved by the fully fixed flat carding machine can improve the yarn hairiness index to a certain extent, while the subtle changes in the short fiber content caused by carding differences fail to form statistically valid inter-group disparities. It is indicated that the difference in the carding scheme has a limited comprehensive effect on the final yarn hairiness.

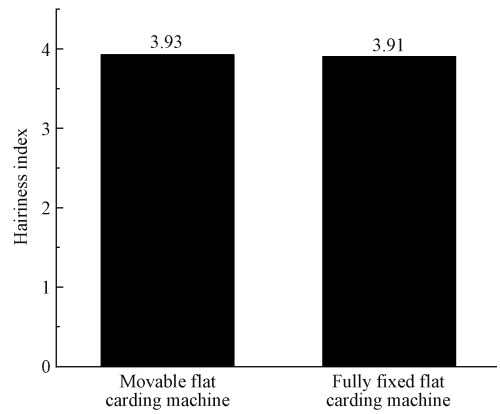


Fig. 8 Comparison of average yarn hairiness index

Table 5 Results of hairiness statistical analysis

Parameter	Degree of freedom	Significance
Hairiness index	35.69	0.436

3.4 Analysis of nep counts

The average nep counts of yarns processed by the fully fixed flat carding machine and movable flat carding machine are presented in Fig. 9, and the corresponding independent-sample *t*-test results are shown in Table 6. For example, nep + 140% is defined as a cotton nep whose cross-sectional mass exceeds the nominal linear density by more than 140%. It is demonstrated that no statistically significant differences are observed in the counts of nep + 140%, nep + 200%, and nep + 280% between the two carding schemes. Nep formation is predominantly determined by the inherent entanglement state of fibers[17-18]. Chemical fibers feature smooth surfaces, low friction coefficients, and no natural crimp, so the variation in fiber straightness, parallelism and separation degree caused by different carding schemes hardly induces substantial nep generation. This fundamental fiber characteristic accounts for the insignificant inter-group differences in nep counts under different carding conditions.

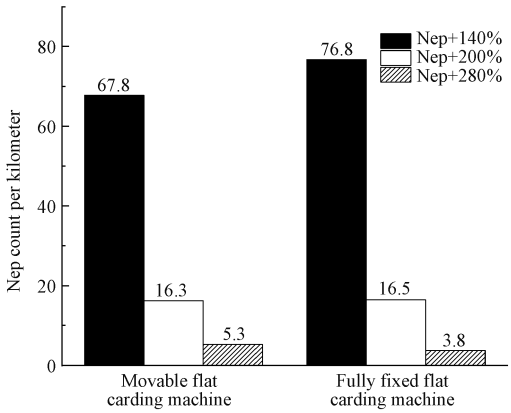


Fig. 9 Comparison of average yarn nep counts

Table 6 Statistical analysis of nep counts

Parameter	Degree of freedom	Significance
Nep+140%	37. 996	0. 160
Nep+200%	37. 854	0. 934
Nep+280%	37. 723	0. 313

3. 5 Analysis of tensile properties

According to the data presented in Fig. 10 and Table 7, no statistically significant differences in the yarn tenacity and elongation at break are observed between yarns produced by the fully fixed flat carding machine and movable flat carding machine, indicating that variations in card clothing structures have no prominent effect on the yarn tensile properties. The yarn tenacity is primarily determined by the inherent fiber strength, interfiber cohesion, and the number of fractured fibers under loading.

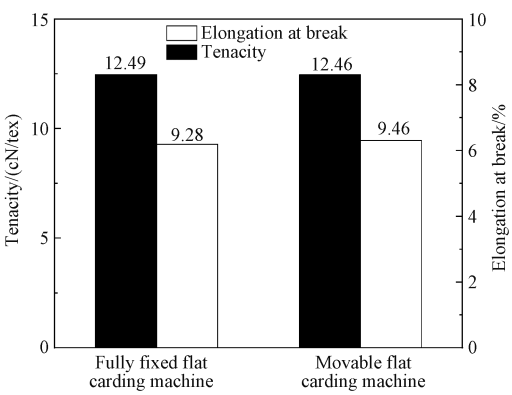


Fig. 10 Comparison of average tensile properties

Table 7 Statistical analysis of tensile properties

Parameter	Degree of freedom	Significance
Tenacity	38. 000	0. 555
Elongation at break	30. 984	0. 110

The sliver nep count and short-fiber content by number exhibit no significant inter-group differences in this study, demonstrating that different card clothing structures do not induce obvious fiber damage, thereby resulting in insignificant variations in yarn tensile properties. Elongation at break is closely related to the synchronous extension behavior of internal fibers, where uniform fiber deformation can avoid premature fracture caused by the localized uneven stress. Nevertheless, the five-component blended yarn in this study possesses diverse fiber properties, and such inherent differences weaken the potential improvement in fiber deformation consistency brought by airflow optimization, ultimately leading to no significant distinction in the yarn elongation at break between the two schemes.

4 Conclusions

This work investigates the influence of airflow distribution on carding blended fibers by two carding machines through numerical simulation. The velocity distribution contour reveals that the airflow boundary layer generated by the fully fixed flat carding machine is narrower than that by the movable flat carding machine in both the axial direction of the cylinder and the vertical dimension. This airflow configuration yields multiple beneficial effects, including reduced nep formation, enhanced carding intensity, and improved fiber alignment and parallelism. Subsequent validation through the production of diacetate/viscose/heat-shrinkable acrylic/micro-denier acrylic/wool blended yarns confirmed the simulation results, with significant reductions in yarn CVm and thin place −40% observed, demonstrating the potential of fully fixed flat carding machines for multi-fiber blending.

References

[1] Bagwan A S A, Jadhav K. Card setting: a factor for controlling sliver quality and yarn [J]. *Journal of Textile Science & Engineering*, 2016, 6(2): 1-3.

[2] Guo D L, Dong Z Q. Development overview of new foreign carding machine and carding technology [J]. *Cotton Textile Technology*, 2015, 43(10): 79-84. (in Chinese)

[3] Sun P Z, Cao J P. Advance in research on entire stationary flat card [J]. *Journal of Textile Research*, 2009, 30(5): 137-141. (in Chinese)

[4] Mandl G. New technology for improved carding [J]. *Melliand English*, 2005(3): 18-21.

[5] He S S, Cheng L D, Xue W L, et al. Three-dimensional numerical simulation of air flow and fiber dynamic in carding region in carding machine [J]. Te*xtile Research Journal*, 2019, 89(19/20): 3916-3926.

[6] He S S, Cheng L D, Xue W L, et al. Card clothing with misaligned teeth for the card: Carding mechanism and application [J]. *Textile*

Research Journal, 2023, 93(1/2): 124-132.
[7] Ou H L. The analysis of the air flow theory of the card and the anatomy of the case [J]. *Textile Accessories*, 2013, 40(6): 6-9. (in Chinese)
[8] Xiao J M, Zeng Y P, Dai X L. Development and use of full-fixed flat carding machine [J]. *Cotton Textile Technology*, 2018, 46(6): 67-73. (in Chinese)
[9] Chen Y F. Process principle and spinning effect analysis on entire stationary flat card [J]. *China Textile Leader*, 2022(3): 80-83. (in Chinese)
[10] Wang H W, Zhang Z Q, Zhao J K, et al. Application effect analysis of full fixed flat carding machine [J]. *Cotton Textile Technology*, 2023, 51(4): 48-52. (in Chinese)
[11] Jin X, Gu Y J. Development of diacetate fiber and modal blended knitted home-wear fabric [J]. *Knitting Industries*, 2024(2): 5-8. (in Chinese)
[12] Pavlov T. Textile airflow problems[M]. Zhou C N, Xing Y S, trans. Beijing: China Textile & Apparel Press, 1988. (in Chinese)
[13] Liu R, Wang B. Cotton spinning test[M]. 3rd ed. Beijing: China Textile & Apparel Press, 2008. (in Chinese)
[14] Cao J P, Zhang Z D, Zhang M G, et al. Correlation analysis on relationship between short fiber content of card sliver and yarn parameters [J]. *Journal of Textile Research*, 2018, 39(12): 30-36. (in Chinese)
[15] Hossain M A, Haque M S, Mohiuddin M, et al. A novel approach to produce neppy yarn in vortex spinning technology [J]. *The Journal of the Textile Institute*, 2025, 116(1): 1-11.
[16] Wu D Y. The cause and control of yarn hairiness [J]. *China Fiber Inspection*, 2018(12): 133-134. (in Chinese)
[17] Ou H L. The cause and control of the hairiness of the ring spun yarn [J]. *Textile Accessories*, 2013, 40(3): 22-26.
[18] Li X L, Yang Q Y. Factor analysis of affecting regenerated cellulose fiber carding quality [J]. *Cotton Textile Technology*, 2022, 50(5): 48-52. (in Chinese)

全固定盖板多元纤维混合梳理理论与实践

宋欣语[1]，戴美磊[2]，张书峰[3]，薛文良[1*]，程隆棣[1]

1. 东华大学 纺织学院，纺织面料技术教育部重点实验室，上海 201620
2. 浙江锦峰纺织机械有限公司，浙江 温州 325041
3. 山东联润新材料科技有限公司，山东 枣庄 277400

摘　要：为探究全固定盖板梳棉机与活动盖板梳棉机在分梳效率上的差异，本研究采用 Fluent 软件对两类机型锡林-盖板间的气流速度分布进行数值模拟，重点分析了针齿微观区域的气流形态特征。通过实际生产二醋酸/黏胶/热收缩腈纶/细旦腈纶/羊毛混纺纱线，对多元纤维混合梳理的模拟结果进行了验证。结果表明：全固定盖板梳棉机在针齿附近形成的气流边界层更稳定，且这种气流分布特征能提升分梳效率。

关键词：梳棉机；全固定盖板；多元纤维混合；模拟